NASA Technical Memorandum **107591**

# COMPUTATIONAL METHODS FOR GLOBAL/LOCAL ANALYSIS

Jonathan B. Ransom
NASA Langley Research Center
Hampton, VA 23665

Susan L. McCleary
Lockheed Engineering & Sciences Company
Hampton, VA 23666

Mohammad A. Aminpour
Analytical Services & Materials, Inc.
Hampton, VA 23666

Norman F. Knight, Jr.
Clemson University
Clemson, SC 29634

**August 1992**

# NASA
National Aeronautics and
Space Administration

**Langley Research Center**
Hampton, Virginia 23665

N92-33104

Unclas

G3/39   0120897

(NASA-TM-107591) COMPUTATIONAL
METHODS FOR GLOBAL/LOCAL ANALYSIS
(NASA)   24 p
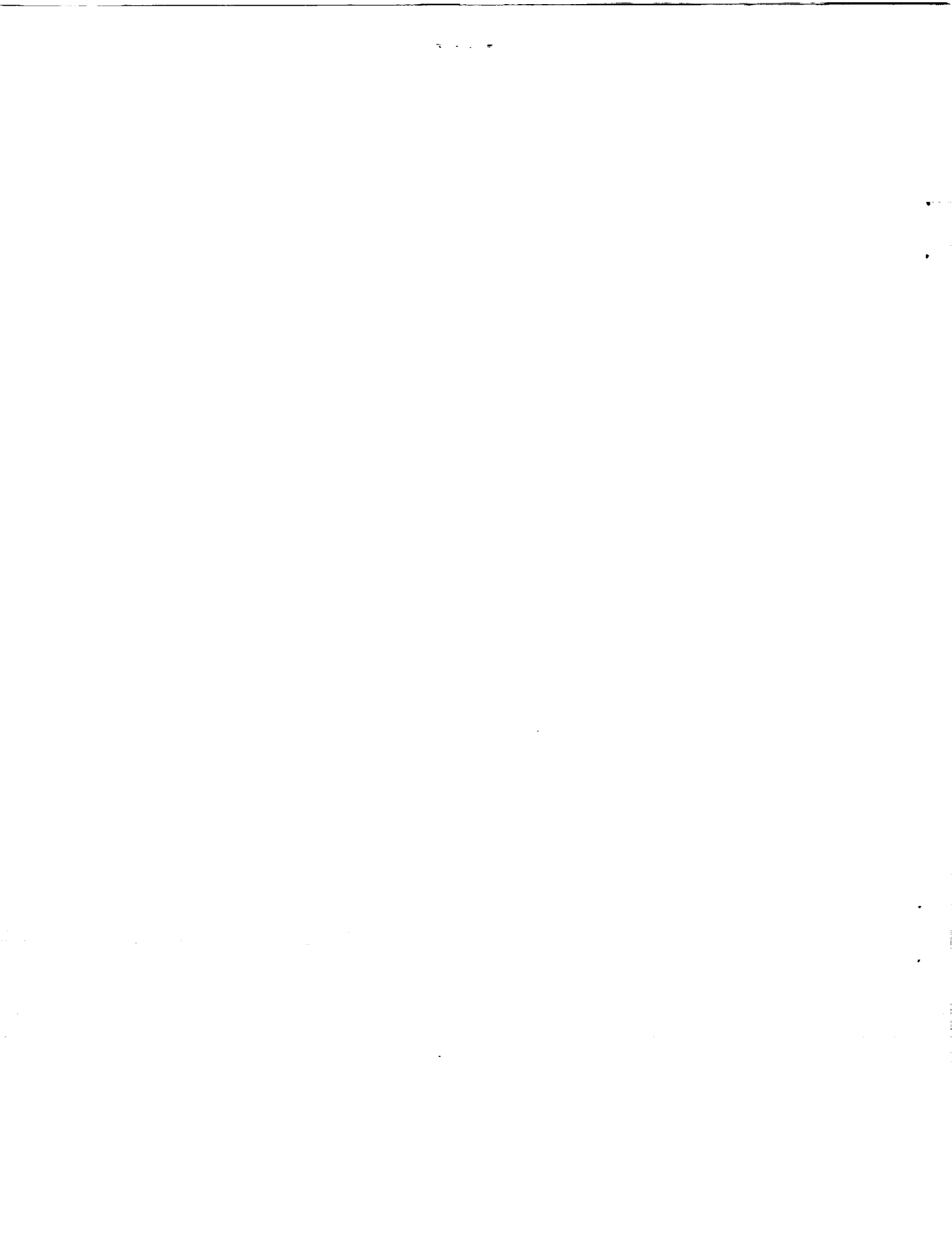
# Computational Methods for Global/Local Analysis†

Jonathan B. Ransom‡, Susan L. McCleary*, Mohammad A. Aminpour**
NASA Langley Research Center
Hampton, Virginia 23665-5225
and
Norman F. Knight, Jr.***
Clemson University
Clemson, South Carolina 29634-0921

## Abstract

Computational methods for global/local analysis of structures which includes both uncoupled and coupled methods are described. In addition, global/local analysis methodology for automatic refinement of incompatible global and local finite element models is developed. Representative structural analysis problems are presented to demonstrate the global/local analysis methods.

## Introduction

The use of composite materials in the design of aircraft structures introduces analytical complexity due to the nature of the material systems and their failure modes. Moreover, new structural concepts introduce additional modeling complexity due to the details of material and geometric discontinuities. Predicting the strength of these structural configurations requires an accurate stress analysis capability. However, detailed analysis of complex aircraft structures can severely tax even today's computing environment. Therefore, it is highly desirable to utilize detailed modeling only where necessary. Embedding local refinement in a single model of the entire structure may lead to highly complex modeling due to the use of transition modeling between highly-refined regions and regions with less refinement. In addition, transition modeling typically introduces distorted elements into the finite element model which may adversely affect the accuracy of the solution. Thus, global/local methods which use different idealizations in different structural regions (i.e., global and local regions) have been used to determine the detailed response of structures. These global/local methods often reduce modeling complexity, however, some of them still require at least some level of transition modeling between the highly-refined and less-refined finite element meshes (refs. 1 to 4). For the methods using transition modeling, one-to-one nodal correspondence is required on the boundaries of the global and local models. Such nodal correspondence will hereafter be referred to as nodal compatibility.

Global/local methods which do not require such nodal compatibility along common subdomain boundaries provide the desirable feature of modeling flexibility and eliminate the need

---

† Invited Talk at the 1992 ASME Summer Mechanics and Materials Meeting, Arizona State University, Tempe, AZ, April 28 - May 1 , 1992.

‡ Aerospace Engineer, Computational Mechanics Branch, Structural Mechanics Division.

* Senior Engineer, Lockheed Engineering and Sciences Company.

** Research Scientist, Analytical Services and Materials, Inc.

*** Associate Professor, Department of Mechanical Engineering.

for transition modeling. These methods fall into one of two categories. In the first category, results from a relatively coarse model are interpolated and applied as boundary conditions (*i.e.,* displacements or forces) on an independent detailed local model of the region of interest (see, for example, refs. 5 and 6). Thus, methods in this category are considered uncoupled and are advantageous when the region of interest is not known prior to or not adequately modeled in the initial global analysis. However, typically no provision is made for interaction between the global and local models.

In the second category, the detailed refinement is incorporated within the global model. Methods in this category are considered coupled and provide modeling flexibility (*i.e.,* they permit independent modeling of the global and local regions) as well as a coupling of the global and local analyses (*i.e.,* they provide the necessary interaction between the global and local models). Examples of coupled methods include domain decomposition and coupling techniques which focus on the development of such methods for parallel computers (refs. 7 and 8). Other methods use some form of multi-point constraints along the global and local boundary (refs. 9 and 10).

The purpose of this paper is to describe two methods, one in each of the previously discussed categories, that have been developed for global/local analysis. These methods, which include both uncoupled (ref. 11) and coupled (ref. 12) global/local methods, have been implemented in a general-purpose finite element code, COMET (ref. 13). Both methods eliminate the need for transition modeling and nodal compatibility across the common boundary between the local and global models. The uncoupled global/local method uses surface spline interpolation to determine the boundary conditions for the incompatible local model. The coupled global/local method uses an independent function along the interface between the subdomains to couple the incompatible global and local subdomains. In addition, an error detection and control strategy has been combined with the coupled global/local analysis method to automatically refine the independently discretized regions. The description of each of these global/local analysis methods including their mathematical formulations is presented first. Then, the methods are demonstrated on selected linear, static structural analysis applications.

## Global/Local Analysis Methods

Global/local analysis procedures which determine the detailed response of structures using different idealizations in specific regions are described in this section. Two computational methods are described: (1) an uncoupled global/local analysis method and (2) a coupled global/local analysis method. In addition, an error detection and control strategy (refs. 14 and 15) is described and is combined with the coupled global/local analysis method in order to automatically refine selected independently discretized structural regions. All methods have been implemented in a common structural analysis framework (refs. 13 and 17).

### Uncoupled Global/Local Method

The uncoupled global/local analysis method was developed in detail in reference 11 and is briefly described herein. The method employs spline interpolation functions which satisfy the linear plate bending equation to determine "boundary conditions" for the local model. A schematic which describes the uncoupled global/local analysis method is shown in figure 1. The global analysis is performed first. The interpolation region encompassing the critical

region is specified. A surface spline interpolation function is evaluated at every node in the interpolation region. The displacement field from the global analysis is used to compute the unknown coefficients of the surface spline function. An independent, more refined, local model is generated within the previously–defined interpolation region. The interpolated displacement field is used to produce a local displacement field which is applied as a "boundary condition" on the boundary of the local model. Then, an independent, two–dimensional local finite element analysis is performed.

This method can be used to determine local two-dimensional stress states for specific structural regions using independent, refined local models which exploit information provided by less-refined global models. The method does not require knowledge of the regions requiring local detailed stress analysis in advance. However, the analyst may be able to anticipate which regions will experience high stresses and the global model can be developed with this knowledge in mind. In addition, transition modeling is eliminated since independent global and local models are used.

One of the key components of this global/local method is the interpolation of the global solution to determine boundary conditions for the local model. The interpolation is performed using a surface spline approach. A surface spline is used to interpolate a function of two variables and removes the restriction of single variable schemes which require a rectangular array of grid points. The derivation of the surface spline interpolation function used herein is based on the classical plate bending equation

$$DV^4 w(x, y) = q(x, y). \tag{1}$$

where $D$ is the flexural rigidity, $q(x, y)$ is the transverse loading and $w(x, y)$ is the transverse deflection of the plate. It ia assumed that $q(x, y) = \sum_{i=1}^{n} \frac{p_i}{16\pi D} \delta(x - x_i, y - y_i)$, where $n$ is the number of nodes in the interpolation region, $p_i$ is the applied point load at the $i^{th}$ node in the region and $\delta(x - x_i, y - y_i)$ is the two-dimensional Dirac delta function such that $\delta(x - x_i, y - y_i) = 1$, when $x = x_i$ and $y = y_i$; and $\delta(x - x_i, y - y_i) = 0$, otherwise. The interpolation function, $w(x, y)$, may be written as

$$w(x, y) = a_0 + a_1 x + a_2 y + a_3 x^2 + a_4 xy + a_5 y^2 + a_6 x^3 + a_7 x^2 y +$$

$$a_8 xy^2 + a_9 y^3 + \sum_{i=1}^{n} F_i r_i^2 \ln(r_i^2) \tag{2}$$

where

$$r_i^2 = (x - x_i)^2 + (y - y_i)^2, \tag{3}$$

$F_i = \frac{p_i}{16\pi D}$, and $x_i, y_i$ are the coordinates of the $i^{th}$ node in the interpolation region. The logarithmic term, $r_i^2 \ln(r_i^2)$, in equation (2) is the fundamental solution of equation (1) for a unit point load at the $i^{th}$ node in the interpolation region. This type of interpolation was first used by Harder and Desmarais (ref. 16) to interpolate pressure loads on idealized wing structures. For that application, only three constants $a_0$, $a_1$, and $a_2$ were used. In reference 11, a complete cubic polynomial was used for general structural applications. The $n + 10$ unknown spline interpolation coefficients $(a_0, a_1, a_2, \ldots, a_9, F_i)$ are determined by evaluating equation (2)

at $n$ nodes and solving the resulting equations along with the following additional ten constraint equations:

$$\sum_{i=1}^{n} F_i = 0 \qquad \sum_{i=1}^{n} F_i y_i^2 = 0$$

$$\sum_{i=1}^{n} F_i x_i = 0 \qquad \sum_{i=1}^{n} F_i x_i^3 = 0$$

$$\sum_{i=1}^{n} F_i y_i = 0 \qquad \sum_{i=1}^{n} F_i x_i^2 y_i = 0 \tag{4}$$

$$\sum_{i=1}^{n} F_i x_i^2 = 0 \qquad \sum_{i=1}^{n} F_i x_i y_i^2 = 0$$

$$\sum_{i=1}^{n} F_i x_i y_i = 0 \qquad \sum_{i=1}^{n} F_i y_i^3 = 0$$

These constraint equations are used to prevent equation (2) from becoming unbounded for large values of $x$ and $y$. The matrix equation is formed by combining equations (2) and (4), namely

$$\begin{bmatrix} \boldsymbol{\Omega} & \mathbf{P} \\ \mathbf{P^T} & \mathbf{0} \end{bmatrix} \begin{bmatrix} \mathbf{F} \\ \mathbf{a} \end{bmatrix} = \begin{bmatrix} \mathbf{w} \\ \mathbf{0} \end{bmatrix} \tag{5}$$

where $\mathbf{P}$ is an $n \times 10$ submatrix with the $i^{th}$ row expressed as

$$\mathbf{P}_i = \lfloor 1 \quad x_i \quad y_i \quad x_i^2 \quad x_i y_i \quad y_i^2 \quad x_i^3 \quad x_i^2 y_i \quad x_i y_i^2 \quad y_i^3 \rfloor,$$

$\mathbf{0}$ is a $10 \times 10$ null submatrix, $\boldsymbol{\Omega}$ is an $n \times n$ submatrix with its elements given by

$$\Omega_{ij} = \begin{cases} r_{ij}^2 \ln(r_{ij}^2), & i \neq j \\ 0, & i = j \end{cases} \qquad i, j = 1, 2, \ldots, n$$

The subvectors $\mathbf{a}$ and $\mathbf{F}$ contain the unknown coefficients of the interpolation function, and the subvector $\mathbf{w}$ contains the generalized displacement field from the interpolation region in the global model. The second set of the equations in equation (5), $\mathbf{P^T F} = \mathbf{0}$, is the matrix form of the constraint equations defined by equations (4). Upon solving equation (5) for the coefficients $(a_0, a_1, a_2, \ldots, a_9, F_j)$, equation (2) is evaluated at the $l$ nodes along the global/local interface boundary to obtain the interpolated data at the boundary nodes of the local model and is given by

$$w_{g/l}(x_i, y_i) = a_0 + a_1 x_i + a_2 y_i + a_3 x_i^2 + a_4 x_i y_i + a_5 y_i^2 + a_6 x_i^3 + a_7 x_i^2 y_i +$$

$$a_8 x_i y_i^2 + a_9 y_i^3 + \sum_{j=1}^{n} F_j r_{ij}^2 \ln(r_{ij}^2); \qquad i = 1, 2, \ldots, l. \tag{6}$$

4

If a boundary node of the local model coincides with a node in the interpolation region of the global model, this node corresponds to a "knot" in the surface spline and thus, the interpolated value is exact. Although equation (6) is derived from the classical plate bending equation, it may be used to interpolate each displacement component $u, v$, and $w$, independently. The rotations $\theta_x$, $\theta_y$, and $\theta_z$ are interpolated (using eq. (6)) from the rotations in the interpolation region in the global model instead of differentiating the out-of-plane-deflection, $w$, to obtain the rotations (e.g., $w_{,x}$).

Guidelines for the use of the uncoupled global/local method are presented in reference 11. In this reference, it was shown that the local model boundary should be outside the local gradient in order to obtain smooth stresses across the global/local boundary. However, even if this requirement is not satisfied, the method provides insight of the local behavior. While the method permits simpler modeling than embedding local refinement in a single model analysis, it does not take into account any interaction between the global and local models. Thus, an alternative method which couples the global and local models together has been developed.

## Coupled Global/Local Analysis Method

This coupled global/local analysis method (see fig. 2) was developed in detail in reference 12 and is briefly described herein. In this coupled method, the incompatible global and local models are coupled using an independent function along the interface between subdomains. The global and local subdomains are discretized by independent finite element meshes. The interface, $S$, (see fig. 3) between the subdomains is discretized independently. The displacement field along the interface is expressed in terms of the generalized displacements along the interace.

The modeling flexibility provided by such a method allows an analyst to incorporate local changes in structural design (e.g., hole size and shape) by interchanging different local models within the same global model. Moreover, the method may also be advantageous when combined with adaptive refinement strategies. The use of such nodally incompatible models also minimizes mesh distortion by avoiding skewed elements otherwise necessary in transition modeling.

The method described herein may generally be applied to an arbitrary number of independently modeled regions. However, in the following discussion, the mathematical formulation will be described in terms of two regions and a multi-segmented interface. A two-dimensional domain $\Omega$ is modeled as two independently discretized subdomains, $\Omega_1$ and $\Omega_2$, as shown in figure 3. The interface, $S$, is modeled as semi-independent straight line segments which conform to the configuration but not the discretization of either of the subdomains. Each segment of the interface, $S$, is discretized as a mesh of evenly spaced "pseudo-nodes." In this paper, the following notation conventions are used. The superscript, $i$, is associated with the interface degrees of freedom of a subdomain, and the superscript, $o$, is associated with the other degrees of freedom, not on the interface. The subscript, $j$, denotes the subdomain (e.g., $j = 1, 2$ for the model in fig. 3). Along the $k^{th}$ segment of the interface, S, there are $m_{kj}$ interface nodes for subdomain $j$ and $n_k$ pseudo-nodes on the interface, $S$. Furthermore, it is assumed that each node has $p$ degrees of freedom so that there are $pm_{kj}$ degrees of freedom for the interface nodes of the subdomain $j$ and $pn_k$ degrees of freedom for the interface, $S$.

While three different interface formulations were examined in reference 12, only one is presented herein, namely, the hybrid variational formulation. The displacement field, **v**, along segment $k$ of the interface may be written as

$$\mathbf{v} = \mathbf{Tq}_s \tag{7}$$

where , $\mathbf{T}$ is a $p \times pn_k$ matrix containing the interpolating functions, and $\mathbf{q}_s$ is a vector of $pn_k$ generalized displacements associated with the $n_k$ interface pseudo-nodes. The specific form of $\mathbf{T}$ depends on the type of function chosen to describe the displacement vector, $\mathbf{v}$, and the number of evenly spaced pseudo-nodes, $n_k$, selected along segment $k$ of the interface, $S$. In reference 12, three different functions were examined: linear, quadratic and cubic splines. The cubic spline is used in this study. Equation (7) is assumed to be valid along each segment (segments AB and BC in fig. 3); at the interface corner (point B in fig. 3), the values from each interface segment are constrained to be the same.

The hybrid variational formulation uses an integral form for the compatibility between the interface and the subdomains. The augmented total potential energy is defined as

$$\Pi = \Pi_{\Omega_1} + \Pi_{\Omega_2} + \int_S \boldsymbol{\lambda}_1^T (\mathbf{v} - \mathbf{u}_1) ds + \int_S \boldsymbol{\lambda}_2^T (\mathbf{v} - \mathbf{u}_2) ds \tag{8}$$

where $\boldsymbol{\lambda}_j$ is a vector of Lagrange multipliers and $\mathbf{u}_j$ is the displacement vector along the interface for the subdomain $j$. The total potential energy of subdomain $j$, $\Pi_{\Omega_j}$, is given by

$$\begin{aligned} \Pi_{\Omega_j} &= \frac{1}{2} \mathbf{q}_j^T \mathbf{K}_j \mathbf{q}_j - \mathbf{q}_j^T \mathbf{f}_j \\ &= \frac{1}{2} \lfloor \mathbf{q}_j^{i\,T} \quad \mathbf{q}_j^{o\,T} \rfloor \begin{bmatrix} \mathbf{K}_j^{ii} & \mathbf{K}_j^{io} \\ \mathbf{K}_j^{oi} & \mathbf{K}_j^{oo} \end{bmatrix} \begin{bmatrix} \mathbf{q}_j^i \\ \mathbf{q}_j^o \end{bmatrix} - \lfloor \mathbf{q}_j^{i\,T} \quad \mathbf{q}_j^{o\,T} \rfloor \begin{bmatrix} \mathbf{f}_j^i \\ \mathbf{f}_j^o \end{bmatrix} \quad ; \quad j = 1, 2 \end{aligned} \tag{9}$$

where the generalized displacement vectors $\mathbf{q}_j$, generalized force vectors $\mathbf{f}_j$, and the stiffness matrices $\mathbf{K}_j$, are partitioned into subvectors and submatrices corresponding to *interface* nodes and *other* (non-interface) nodes.

The constraint integrals in equation (8) are added to the functional to enforce, in the variational sense, continuity of displacements across the interface. Equation (8) corresponds to the "double layer interface" or "frame" method of the hybrid variational principal (ref. 18). In this formulation, the Lagrange multipliers, $\boldsymbol{\lambda}$, are assumed independently at the interface for each element, and the displacement vector, $\mathbf{v}$, is assumed independently on the interface, $S$.

Assuming that the displacement boundary conditions are satisfied, the stationary condition for the total potential energy for arbitrary $\mathbf{u}$ in the subdomains, arbitrary $\mathbf{v}$ on the interface, $S$, and arbitrary $\boldsymbol{\lambda}$ on the interface parts of the subdomains, results in the following Euler equations associated with the interface

$$\delta\Pi = 0 \quad \Rightarrow \quad \begin{cases} \boldsymbol{\lambda}_j = (\boldsymbol{\sigma}\mathbf{n})_j; & j = 1, 2 \\ \boldsymbol{\lambda}_1 + \boldsymbol{\lambda}_2 = 0 & \\ \mathbf{u}_j = \mathbf{v}; & j = 1, 2 \end{cases} \quad \text{on } S \tag{10}$$

These equations are in addition to the usual Euler equations which satisfy the equilibrium equations, traction boundary conditions, and the interelement traction continuity. Thus, $\boldsymbol{\lambda}_j$ represents the tractions on the interface and the sum of the tractions across the interface is zero (*i.e.*, equilibrium is maintained across the interface). The dispacements, $u_j$, along the interface

6

of the subdomains is expressed in terms of unknown nodal displacements, $q_j^i$, as $\mathbf{u}_j = \mathbf{N}_j \mathbf{q}_j^i$, and, the Lagrange multipliers, $\boldsymbol{\lambda}_j$, are expressed in terms of unknown coefficients, $\boldsymbol{\alpha}_j$, as $\boldsymbol{\lambda}_j = \mathbf{R}_j \boldsymbol{\alpha}_j$, where $\mathbf{N}_j$ and $\mathbf{R}_j$ are matrices of interpolation functions. The interpolation functions in the matrix $\mathbf{R}_j$ are taken to be constants for linear elements and linear for quadratic elements. Substituting these assumptions into equation (8) and taking the first variation of the potential energy with respect to the independent variables, $\mathbf{q}_j^i, \mathbf{q}_j^o, \mathbf{q}_s$, and $\boldsymbol{\alpha}_j$, and setting it to zero yields the following system of equations:

$$
\begin{bmatrix}
\mathbf{K}_1^{ii} & \mathbf{K}_1^{io} & 0 & 0 & 0 & \mathbf{M}_1 & 0 \\
\mathbf{K}_1^{oi} & \mathbf{K}_1^{oo} & 0 & 0 & 0 & 0 & 0 \\
0 & 0 & \mathbf{K}_2^{ii} & \mathbf{K}_2^{io} & 0 & 0 & \mathbf{M}_2 \\
0 & 0 & \mathbf{K}_2^{oi} & \mathbf{K}_2^{oo} & 0 & 0 & 0 \\
0 & 0 & 0 & 0 & 0 & \mathbf{G}_1 & \mathbf{G}_2 \\
\mathbf{M}_1^T & 0 & 0 & 0 & \mathbf{G}_1^T & 0 & 0 \\
0 & 0 & \mathbf{M}_2^T & 0 & \mathbf{G}_2^T & 0 & 0
\end{bmatrix}
\begin{bmatrix}
\mathbf{q}_1^i \\
\mathbf{q}_1^o \\
\mathbf{q}_2^i \\
\mathbf{q}_2^o \\
\mathbf{q}_s \\
\boldsymbol{\alpha}_1 \\
\boldsymbol{\alpha}_2
\end{bmatrix}
=
\begin{bmatrix}
\mathbf{f}_1^i \\
\mathbf{f}_1^o \\
\mathbf{f}_2^i \\
\mathbf{f}_2^o \\
0 \\
0 \\
0
\end{bmatrix}
\tag{11}
$$

where $\mathbf{M}_j$ and $\mathbf{G}_j$ are integrals on the interface defined in terms of $\mathbf{R}_j$, $\mathbf{T}$, and $\mathbf{N}_j$ as

$$
\mathbf{M}_j = -\int_S \mathbf{N}_j^T \mathbf{R}_j \, ds \quad \text{and} \quad \mathbf{G}_j = \int_S \mathbf{T}^T \mathbf{R}_j \, ds \quad ; \quad j = 1,2
\tag{12}
$$

### Adaptive Global/Local Analysis Procedure

The adaptive global/local analysis procedure, described by figure 4, is a strategy for automatically refining selected, independently discretized regions of a structure within the context of a linear static analysis. In this method, the error detection and control strategy presented in references 14 and 15 and summarized herein is combined with the coupled global/local method previously described.

Initially, the local and global subdomains are identified and independently discretized. A linear stress analysis is performed using the coupled global/local method. Once a displacement solution has been obtained for the coupled system, the two models are again treated as independent for post-processing. Refinement indicators, based on stress resultants smoothed only within a global or local subdomain, are evaluated, and each subdomain is remeshed as needed. If no elements in either model require refining, the solution strategy stops and reports that solution convergence has been achieved. If either or both models change, a new mesh (or meshes) is (are) generated and a new coupled solution is determined. The global and local models are parametrically generated using the high-level command language in COMET such that automatic refinement of the models is accomplished by automatically changing the discretization parameters. The strategy continues iteratively until either convergence to a user-specified error tolerance is achieved or another user-specified termination criterion is met (e.g., maximum number of mesh iterations or maximum execution time).

The error detection and control strategy includes the definition of error and refinement indicators and the development of a mesh refinement strategy. While several error indicators were considered initially, only two proved to be useful in the work presented in references 14 and 15. The first is an adaptation of the energy norm of the error; the second is based on the

7

standard deviation in the stress resultants at element nodes. The first error indicator is used in the present work and is summarized herein.

The energy norm of the error as proposed by Zienkiewicz and Zhu (ref. 19) has been adapted to plate and shell problems. For the $k^{th}$ element, the energy norm of the error, $\|e_k\|_E$, is defined by

$$\|e_k\|_E^2 = \int_{\Omega_e^k} (S_k^* - S_k')^{\mathrm{T}} \overline{C}_k^{-1} (S_k^* - S_k') d\Omega_e = \int_{\Omega_e^k} \Delta S_k^{\mathrm{T}} \overline{C}_k^{-1} \Delta S_k d\Omega_e \qquad (13)$$

where $S_k$ is a vector of stress resultant components (where an * denotes smoothed values and a ′ denotes discrete finite element values); and $\overline{C}$ is the constitutive matrix that relates stress resultants to reference surface strain components.

As an integrated quantity, the energy norm of the error requires either specific element data (i.e., the element shape functions) or an element-independent generalization. This implementation provides an element-independent generalization which allows for the decoupling of the error analysis from other element-specific functions. The distribution of the difference between the smoothed and the discrete values of the stress resultants, $\Delta S$, over each element is assumed to be described by Lagrangian shape functions. This assumption allows for the evaluation of an element-independent error indicator and provides a common basis for the evaluation of different element types but does not ignore all element-specific features in that discrete element stress resultants are calculated using features of the specific element.

The automatic refinement strategy is based on the local refinement indicators; elements needing to be refined are identified using the local refinement indicator (see ref. 19), $\xi_k$, defined by

$$\xi_k = \frac{e_m}{\|e_k\|_E} \qquad (14)$$

where

$$e_m \equiv \bar{\eta}_{tol} \sqrt{\frac{\|u'\|^2 + \|e\|_E^2}{n_{ele}}}, \qquad (15)$$

$\|u'\|$ is the energy norm of the current finite element solution over each subdomain, $\|e\|_E$ is the energy norm of the error in each subdomain and is defined as the sum of the elemental values, $\|e_k\|_E$, and $n_{ele}$ is the total number of elements. At the start of a specific analysis, the user must specify a value for the percent error in the energy norm which will be acceptable for the given analysis; this user-specified tolerance is denoted $\bar{\eta}_{tol}$. Thus, when $\xi_k$ is less than unity for an element or patch of elements, refinement must occur; when $\xi_k$ is greater than unity for a patch of elements, the patch may be "fused" into a patch containing fewer elements. The "fusion" of elements has not been included as part of the error control strategy in this work.

The error indicator discussed herein requires the definition of a smoothed stress resultant field (which is generally available in most large-scale structural analysis codes) as an approximation to the exact stress resultant field. For simplicity, simple nodal averaging has been used

8

to produce the smoothed solutions for the example cited herein. For all nodes, smoothed stress resultants are given by

$$S^{*}_{\alpha_j} = \frac{1}{n_e} \sum_{l=1}^{n_e} S^{''}_{\alpha_j}$$
(16)

where $S^{*}_{\alpha_j}$ is the smoothed stress component $\alpha$ at node $j$, $n_e$ is the number of elements directly connected to node $j$, and $S^{''}_{\alpha_j}$ is the discrete stress component $\alpha$ at node $j$ from element $l$. At geometric and material discontinuities, the stresses in the same geometric plane or of the same material are smoothed separately. It should be noted that any smoothing algorithm may be used since obtaining the smoothed solution is a separate part of the error detection strategy. When calculating the error and the refinement indicators, it is assumed that a smoothed solution is available.

Automatic mesh refinement may take several forms and need not be fully adaptive. A fully adaptive strategy will refine only those elements identified by the refinement indicators as elements requiring refinement. Automatic mesh refinement encompasses a range of refinement techniques and includes any mesh refinement technique which can be performed with minimal user intervention and which can be performed automatically by the structural analysis software. The present work (as in references 14 and 15), employs uniform and quasi-uniform refinement schemes implemented through a high-level command language facility in COMET.

Uniform refinement methods may be global but are best employed on parameterized finite element models so that only portions of the mesh will be refined and sophisticated data structures are not required. This type of refinement is denoted quasi-uniform refinement. Uniform and quasi-uniform refinements will tend to over-refine the finite element model. The cost per analysis of using such refinement is therefore generally higher than the cost of using a fully adaptive refinement technique. Within the context of a general-purpose code, however, a high-level refinement technique which is easily implemented, requires no complex data structures, and little or no modification to existing software, may well be the technique of choice for many analysts.

## Applications

The effectiveness of the global/local analysis methods described in the previous section is demonstrated by determining the response of two structural analysis problems. First, a graphite-epoxy blade-stiffened panel demonstrates the uncoupled global/local analysis method on a representative aircraft subcomponent with characteristics which often require a global/local analysis capability. These characteristics include a discontinuity, eccentric loading, large displacements, large stress gradients, high in-plane loading and a brittle material system. Second, an orthotropic plate with a central crack demonstrates the coupled global/local analysis method. In addition, the plate with a central crack demonstrates the effectiveness of the adaptive global/local analysis procedure. This problem is characterized by a stress singularity at the crack tips which presents a challenge for both the global/local method and the adaptive procedure.

## Blade-Stiffened Panel with Discontinuous Stiffener

An uncoupled global/local analysis of a composite panel with a discontinuous stiffener was presented in reference 11 and is summarized herein. A linear stress analysis of a flat, blade–stiffened, graphite–epoxy panel loaded in axial compression is performed. The overall panel length is 30 in., the overall width is 11.5 in., the stiffener spacing is 4.5 in., the stiffener height is 1.4 in., and the cutout radius is 1 in. The cross section of the three blade–shaped stiffeners is identical. The loading is uniform axial compression in the $x$-direction. The loaded ends of the panel are clamped and the other sides are free. The material system used for the panel is T300/5208 graphite–epoxy unidirectional tapes with a nominal ply thickness of 0.0055 in. The panel skin is a 25-ply symmetric laminate $\left(\left[\pm 45/0_2/\mp 45/0_3/\pm 45/0_3/\mp 45/0\bar{0}\right]_s\right)$ and the blade stiffeners are 24-ply symmetric laminates $\left(\left[\pm 45/0_{10}\right]_s\right)$.

Based on the results from a coarse global model analysis, two local regions are considered: one near the cutout, and one at the skin-stiffener interface near the edge of the cutout. A four-node quadrilateral shell element (ref. 20) was used in the global and local analyses. This element is based on a displacement formulation and includes rotations about the outward normal axis. The coarse global model has 2316 active degrees of freedom. The local models of the region around the cutout and the skin-stiffener interface have 3456 and 462 active degrees of freedom, respectively. The boundary conditions for both local analyses were obtained using data from the coarse global model analysis. Two interpolation regions were used for each of the local analyses. The first interpolation region, specified in the plane of the panel skin, is used to obtain boundary conditions on the local model boundary of the panel skin. The second interpolation region, specified in the plane of the stiffener, is used to obtain boundary conditions on the local model boundary of the stiffener. The boundary conditions for the panel skin and the stiffener were obtained independently. The displacements and rotations at the skin-stiffener intersection on the local model boundaries were taken as those values obtained for the panel skin.

Contour plots of the longitudinal stress resultant $N_x$ are shown in figure 5 superimposed on the deformed global finite element model and undeformed local finite element models. The distribution of the longitudinal stress resultant $N_x$ in the panel skin normalized by the applied running load $(N_x)_{avg}$ (i.e., applied load divided by the panel width) is shown in figure 6 as a function of the lateral distance from the center of the panel normalized by the radius of the cutout. The solution from a very refined global model is used as the reference solution. This refined global model has the same level of refinement in the local regions as the independent local models and has 8460 active degrees of freedom. The coarse global model solution provides good agreement with the reference solution away from the cutout but underestimates (by 24%) the stress concentration at the edge of the cutout. The local model analysis of the region around the cutout predicts normalized stress resultants within 1.4% of the reference solution in the neighborhood of the cutout. The local model analysis of the skin–stiffener interface region also agrees with the reference solution in predicting a higher gradient than the coarse global model analysis. This method may be used to interrogate any other region of the subcomponent as well.

## Plate with a Central Crack

An orthotropic plate which has a central crack and which is subjected to uniform tension is used to demonstrate the coupled global/local analysis method. This problem is characterized by a stress singularity at the crack tips. The remote tensile loading induces mode I crack deformations. Accurate solutions are available in the literature (ref. 22) for this configuration.

The ratio of the plate half-length to the plate half-width, $\frac{L}{b}$, is 2 (see fig. 7). The ratio of the crack half-length to the plate half-width, $\frac{a}{b}$, ranges from 0.125 to 0.75. It is assumed that the material axes (1,2) are along the coordinate axes $(x,y)$. The ratio of the Young's moduli, $\frac{E_x}{E_y}$, is 0.1. The ratio of the shear modulus to the longitudinal Young's modulus , $\frac{G_{xy}}{E_x}$, is 0.8757 and Poisson's ratio, $\nu_{yx}$, is 0.21. Using the symmetries in the problem, one quarter of the plate is modeled. The local area of interest is first isolated from the larger global model and two separate finite element models (shown in fig. 8) are created: one for the global subdomain which is very coarse, and one for the local subdomain which is considerably more refined to delineate the stress gradient near the crack tip. The finite element nodes of the global and local models do not coincide at the global/local interface. The local model dimension is defined by the parameter, $H$, shown in figure 7. A nine-node Assumed Natural-Coordinate Strain element 21 was used in this problem. This element has five degrees of freedom at each node (i.e., three displacements, two bending rotations and no drilling degrees of freedom) and uses a strain approximation to calculate the element stiffness matrix (which is equivalent to a a stiffness matrix calculated using a selectively directionally reduced order of integration). A linear static analysis is performed using the coupled global/local method to join these two incompatible finite element models.

The stress intensity factors, $K$, were calculated from the relationship

$$K = \sqrt{\frac{G}{c}} \tag{17}$$

where $G$ is the strain-energy release rate and $c$ is a constant defined in terms of the material properties. The strain-energy release rate, $G$, is calculated by the virtual crack-closure technique and for quadratic elements (ref. 23) is defined as

$$G = -\frac{1}{\Delta}[F_j v_{j+2} + F_{j-1} v_{j+1}] \tag{18}$$

where $\Delta$ is the element size at the crack tip, $F_j$ and $F_{j-1}$ are internal forces at the crack tip and one node point ahead of the crack tip, respectively, and $v_{j+1}$ and $v_{j+2}$ are the displacements at the first and second node points behind the crack tip (i.e., on the crack face, see fig. 9). Note that no special element (e.g., quarter-point or other singularity element) is used at the crack tip. The value of $c$ for orthotropic materials is given in reference 24 as

$$c = \left(\frac{A_{11}A_{22}}{2}\right)^{\frac{1}{2}} \left[\sqrt{\frac{A_{22}}{A_{11}}} + \frac{2A_{12} + A_{66}}{2A_{11}}\right]^{\frac{1}{2}} \tag{19}$$

where

$$A_{11} = \frac{1}{E_x}, \quad A_{22} = \frac{1}{E_y}, \quad A_{12} = -\frac{\nu_{yx}}{E_y}, \quad \text{and} \quad A_{66} = \frac{1}{G_{xy}}$$

11

The stress intensity factors, $K$, normalized by $\sigma_0\sqrt{\pi a}$ are shown in figure 10 as a function of the crack half-length to plate half-width ratio, $\frac{a}{b}$. The solid curve in the figure represents the solution by Bowie (ref. 22). The open circles represent the stress intensity factors obtained from the finite element analyses using the coupled global/local method. The calculated stress intensity factors are in excellent agreement with the solution by Bowie (ref. 22).

An adaptive analysis is performed on the plate with a central crack by again isolating the local area of interest from the larger global model and creating two separate finite element models: one for the global subdomain which is initially very coarse, and one for the local subdomain which is also initially coarse. A linear static analysis is again performed using the coupled global/local method to join the two incompatible finite element models. Refinement indicators based on the energy norm of error, with a 5% error tolerance, are evaluated on Model 1 (shown on the upper left of fig. 11 with an enlarged local subdomain). These indicators suggest that refinement of both the global and local models is required (darker shaded elements on the figure indicate that refinement is needed). New models are generated automatically for both global and local subdomains (denoted Model 2 in the center of the upper portion of the figure), an analysis is performed, and refinement indicators are evaluated. In subsequent analyses, refinement is required only in the local subdomain of Models 2 and 3 as shown by the refinement indicators in the figure. A new local model is automatically generated, the global model is allowed to remain the same, and a fourth and final linear analysis is performed on Model 4 (lower left of the figure). Although refinement indicators again suggest that refinement is needed, the solution procedure is terminated. As the mesh becomes more refined in the neighborhood of the crack tip, the solution is driven to an increasingly better representation of the singularity, thus the refinement will continue for this problem until user-terminated. The transverse stress resultant, $N_y$, along the width of the panel at the centerline (along the $x$ axis shown in fig. 7) is shown in figure 12 for each of the four models. The sequence of four models generates increasing values of peak stress as the solution is driven to a better numerical representation of infinity at the crack tip. The stress intensity factors predicted using the four models are shown in figure 13 as a function of the number of degrees of freedom in each model. The stress intensity factor increases and approaches the reference solution by Bowie 22 as the number of degrees of freedom is increased. The stress intensity factor predicted by Model 4 (1605 degrees of freedom) is within 0.1% of the Bowie's solution.

## Concluding Remarks

In summary, two computational methods for global/local analysis of structural components have been described. The methods are uncoupled and coupled global/local analysis methods. Also, methodology for automatic refinement of incompatible global and local models has been developed. The effectiveness of the methods has been demonstrated using selected linear static structural analysis applications.

The uncoupled global/local analysis method presented herein reduces the analyst's computational effort and removes the restriction of having to know the regions requiring local detailed stress analysis in advance. The coupled global/local analysis method provides interaction between the global and local models. Both global/local methods described herein eliminate the need for potentially complex transition modeling from highly-refined regions to regions with less

refinement and thus reduce the modeling effort. The global/local analysis capabilities provide efficient strategies for predicting local detailed stress states using relatively coarse finite element models in the far-field. The error detection and control strategy combined with the coupled global/local analysis method has been shown to be an effective procedure for improving the accuracy of global and local results. The combined procedure provides a modeling technique for automatically refining incompatible global and local models.

The global/local analysis methods described and demonstrated herein, provide techniques for predicting local detailed structural response. In addition, the use of these methods should reduce the analyst's modeling effort and thus, should favorably impact the design process for structural components.

## References

1. Clough, R. W.; and Wilson, E. L.: Dynamic Analysis of Large Structural Systems with Local Nonlinearities. *Computer Methods in Applied Mechanics and Engineering*, vol. 17/18, Part 1, January 1979, pp. 107-129.

2. Anon.: *ANSYS User's Manual.* Swanson Analysis Systems, Inc., Houston, PA, 1979.

3. Whitcomb, J. D.: Iterative Global/Local Finite Element Analysis. *Computers and Structures*, vol 40, no. 4, 1991, pp. 1027-1031.

4. Jara-Almonte, C. C.; and Knight, C. E.: The Specified Boundary Stiffness/Force SBSF Method for Finite Element Subregion Analysis. *International Journal for Numerical Methods in Engineering*, vol. 26, 1988, pp. 1567-1578.

5. Schwartz, D. J.: Practical Analysis of Stress Raisers in Solid Structures. *Proceedings of the $4^{th}$ International Conference on Vehicle Structural Mechanics*, Warrandale, PA, Nov. 1981, pp. 227-231.

6. Kelley, F. S.: Mesh Requirements of a Stress Concentration by the Specified Boundary Displacement Method. *Proceedings of the Second International Computers in Engineering Conference*, ASME, vol. 3, San Diego, CA, Aug. 1982, pp. 39-42.

7. Farhat, C.; and Roux, F. H.: A Method of Finite Element Tearing and Interconnecting and its Parallel Solution Algorithm. *International Journal for Numerical Methods in Engineering*, vol. 32, no. 6, 1991, pp. 1205-1228.

8. Maday, Y.; Mavriplis, C.; and Patera, A.: *Nonconforming Mortar Element Methods: Application to Spectral Discretization.* ICASE Rep. No. 88-59, NASA CR-181729, NASA Langley Research Center, 1988.

9. Schaeffer, H. G.: *MSC/NASTRAN Primer, Static and Normal Modes Analysis.* Schaeffer Analysis, Inc., Mont Vernon, NH, 1979, pp. 262-265.

10. Krishnamurthy, T.; and Raju, I. S.: An Independent Refinement and Integration Procedure in Multiregion Finite Element Analysis. *Proceedings of the AIAA/ASME/ASCE/AHS $33^{rd}$*

*Structures, Structural Dynamics and Materials Conference*, Part 1, Dallas, TX, April 13 - 15, 1992, pp. 302-312. Also AIAA Paper No. 92-2290.

11. Ransom, J. B.; and Knight, N. F., Jr.: Global/Local Stress Analysis of Composite Panels. *Computers and Structures*, vol 37, no. 4, 1990, pp. 375-395.

12. Aminpour, M. A.; Ransom, J. B.; and McCleary, S. L.: Coupled Analysis of Independently Modeled Finite Element Subdomains. *Proceedings of the AIAA/ASME/ASCE/AHS 33$^{rd}$ Structures, Structural Dynamics and Materials Conference*, Dallas, TX, April 13-15, 1992, pp. 109-120. (Available as AIAA Paper No. 92-2235)

13. Stewart, C. B. (Compiler): *The Computational Structural Mechanics Testbed User's Manual*. NASA TM-100644, 1989.

14. McCleary, S. L.: *An Adaptive Nonlinear Analysis Procedure for Plates and Shells*. M.S. Thesis, George Washington University, Hampton, VA, 1990.

15. McCleary, S. L.; and Knight, N. F., Jr.: Error Detection and Control for Nonlinear Shell Analysis. *Proceedings of the Sixth World Congress and Exhibition on Finite Element Methods*, October 1 - 5, 1990. Also NASA TM-102723.

16. Harder, R. L.; and Desmarais, R. N.: Interpolation Using Surface Splines *Journal of Aircraft*, vol 9, no. 2, February 1972, pp. 189-191.

17. Gillian, R. E.; and Lotts, C. G.: *The CSM Testbed Software System – A Development Environment for Structural Analysis Methods on the NAS CRAY-2*. NASA TM-100642, 1988.

18. Zienkiewicz, O. C.: *The Finite Element Method*. Third Edition, McGraw-Hill Book Company, UK, 1977, pp. 304-328.

19. Zienkiewicz, O. C.; and Zhu, J. Z.: A Simple Error Estimator and Adaptive Procedure for Practical Engineering Analysis. *International Journal for Numerical Methods in Engineering*, vol. 24, 1987, pp. 337-357.

20. Almroth, B. O.; Brogan, F. A.; and Stanley, G. M.: *Structural Analysis of General Shells - Volume II: User Instructions for STAGSC-1*. NASA CR-165671, 1981.

21. Park, K. C.; and Stanley, G. M.: A Curved $C^0$ Shell Element Based on Assumed Natural-Coordinate Strains. *ASME Journal of Applied Mechanics*, vol 108, 1986, pp. 278-290.

22. Bowie, O. L.; and Freese, C. E.: Central Crack in Plane Orthotropic Rectangular Sheet. *International Journal of Fracture*, vol. 8, no. 1, 1972, pp. 49-58.

23. Raju, I. S.: Calculation of Strain-Energy Release Rates with Higher Order and Singular Finite Elements. *Engineering Fracture Mechanics*, vol. 28, no. 3, 1987, pp. 251-274.

24. Paris, P. C.; and Sih, G. C.: *Stress Analysis of Cracks*. Special Technical Publication No. 381, American Society for Testing Materials, 1965.
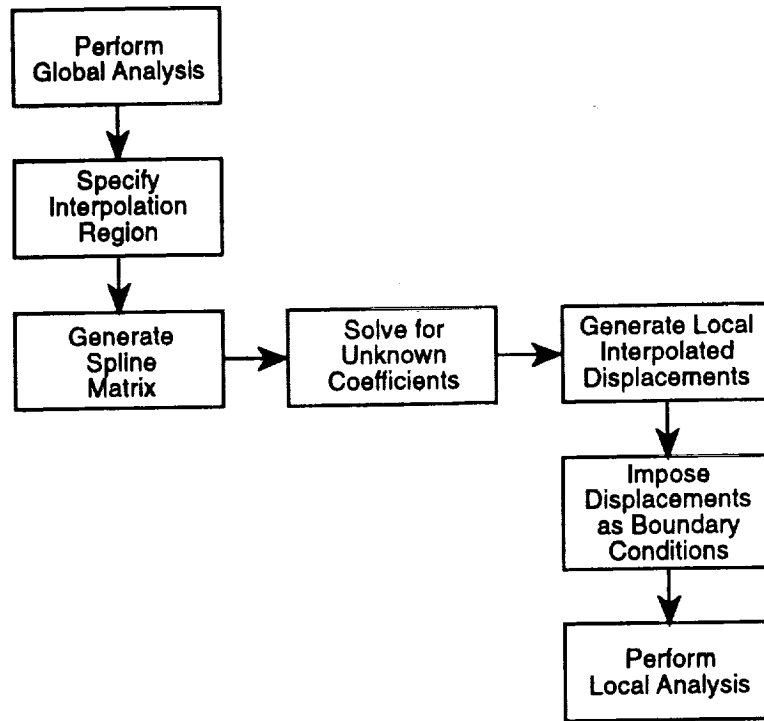
14

Figure 1.   Description of Uncoupled Global/Local Analysis Method.
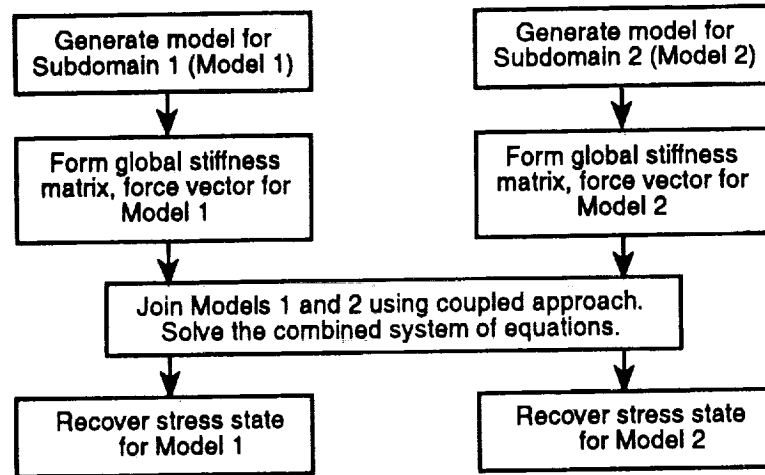


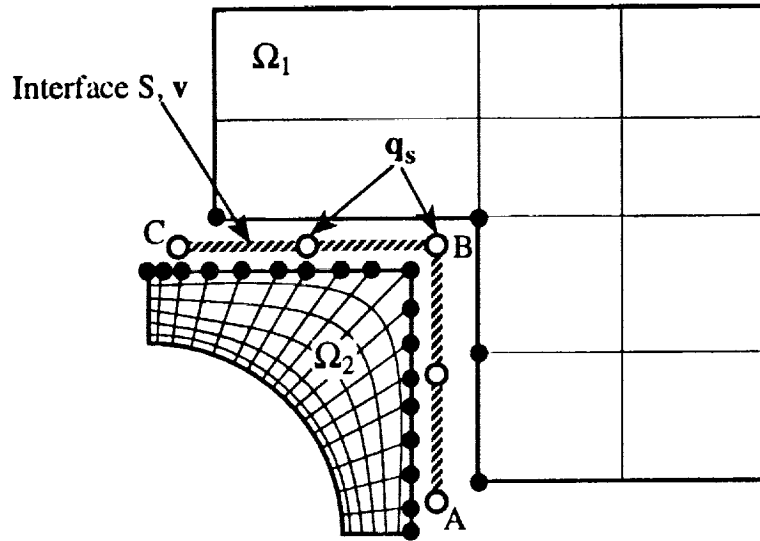Figure 2.   Description of Coupled Global/Local Analysis Method.

15

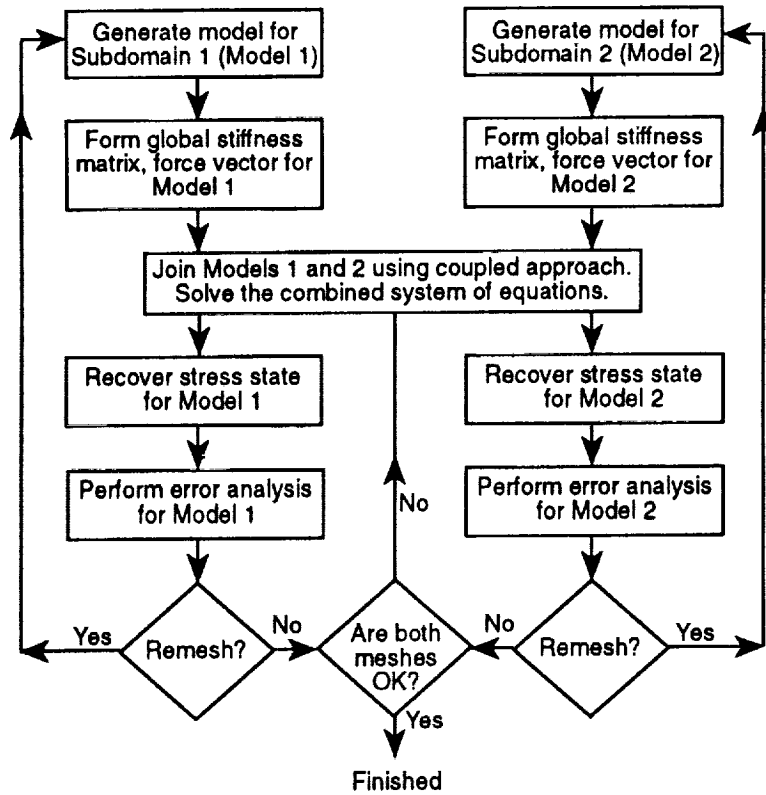Figure 3. Interface Definition for Coupled Global/Local Method.



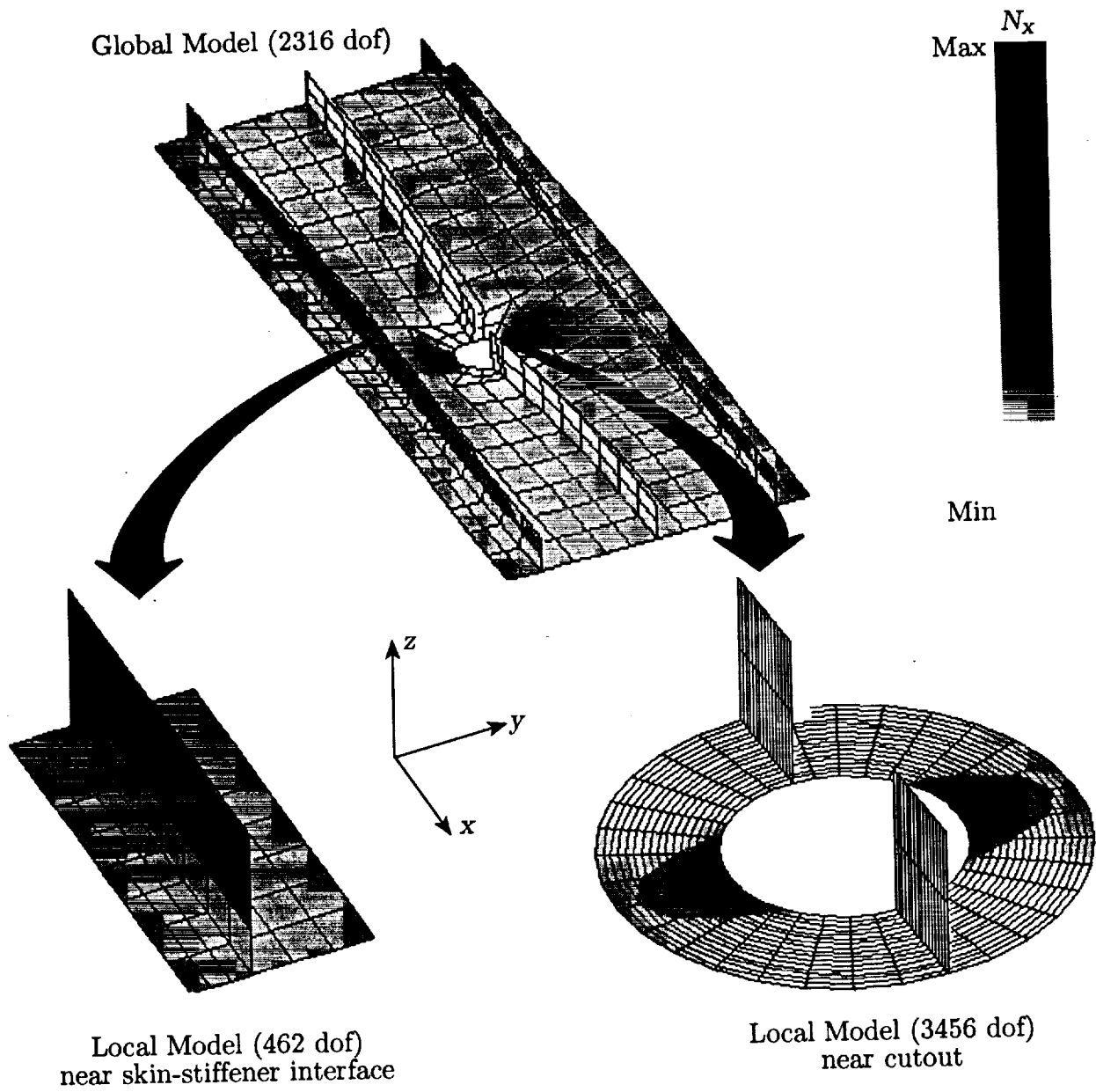Figure 4. Description of Adaptive Global/Local Analysis Method.

Global Model (2316 dof)

$N_x$

Max

Min

Local Model (462 dof)
near skin-stiffener interface

Local Model (3456 dof)
near cutout

Figure 5. Contour Plots of Longitudinal In-plane Stress Resultant, $N_x$.
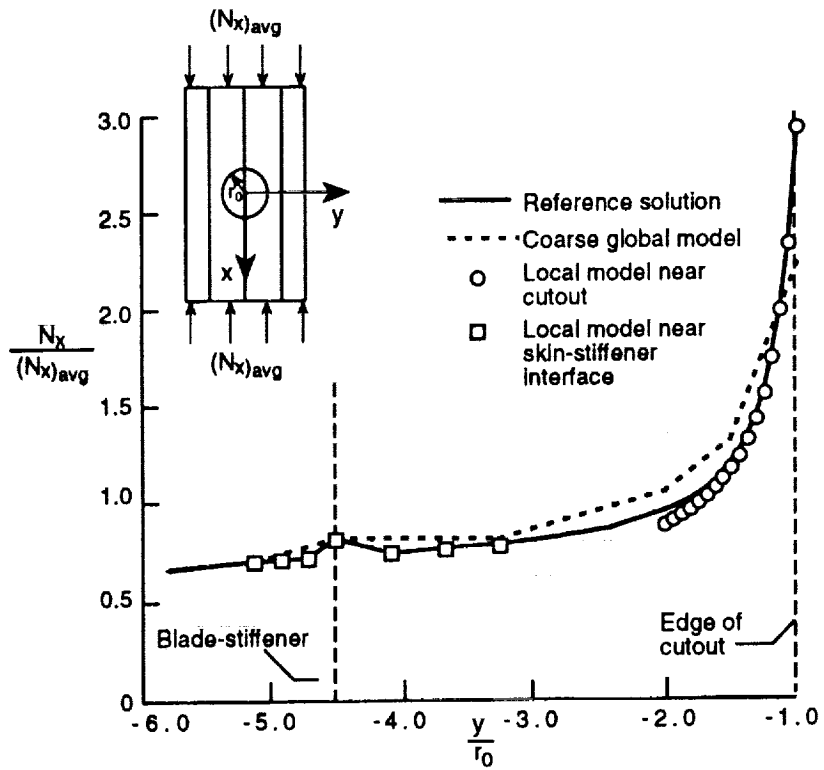
Figure 6.  Longitudinal In-plane Stress Resultant, $N_x$, Distributions.
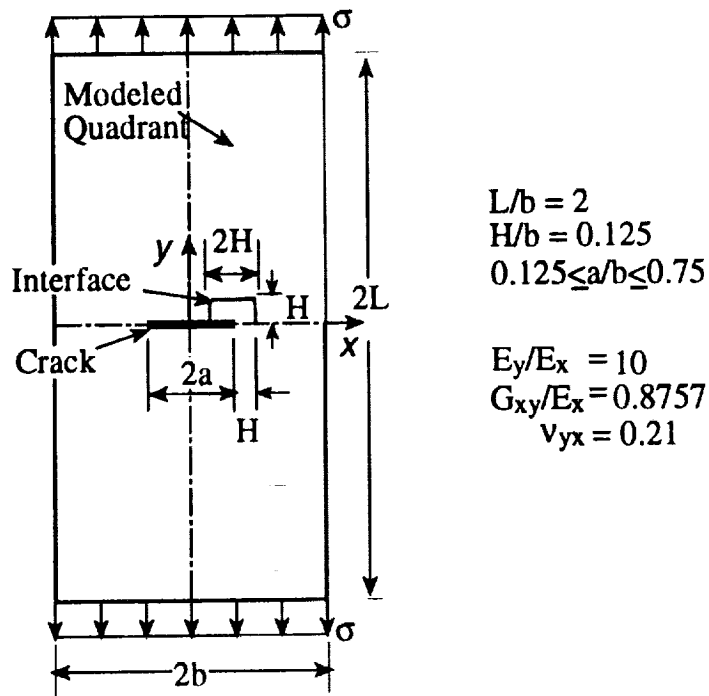
Figure 7. Orthotropic Plate with a Central Crack.

$$L/b = 2$$
$$H/b = 0.125$$
$$0.125 \leq a/b \leq 0.75$$

$$E_y/E_x = 10$$
$$G_{xy}/E_x = 0.8757$$
$$\nu_{yx} = 0.21$$
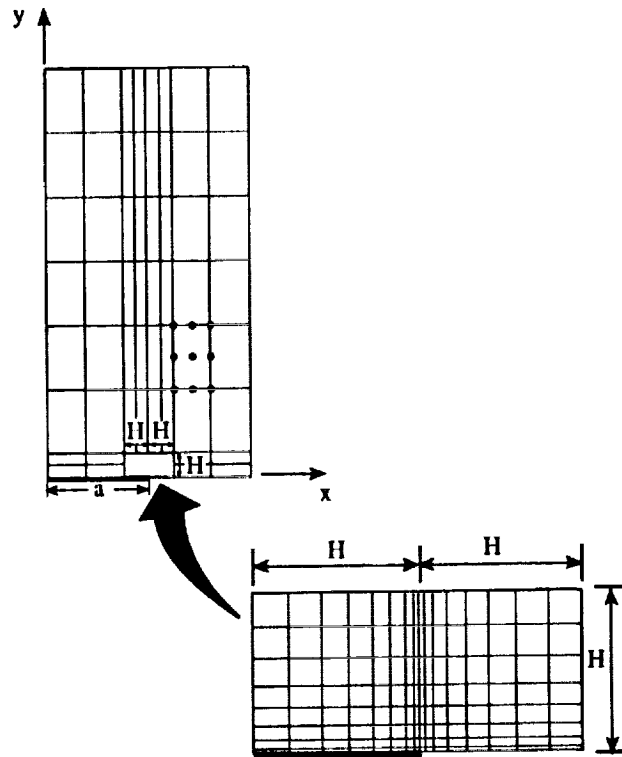


Figure 8. Finite Element Models for One Quadrant of Plate with Central Crack.
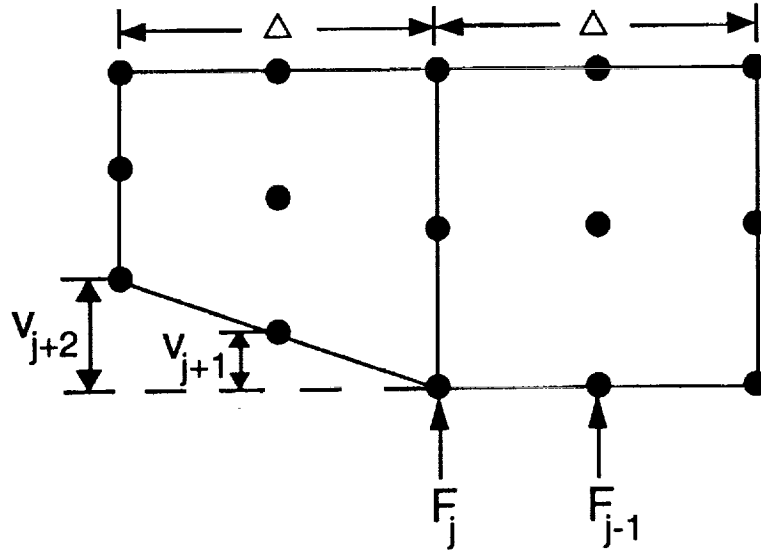
Figure 9. Forces and Displacements near the crack tip.
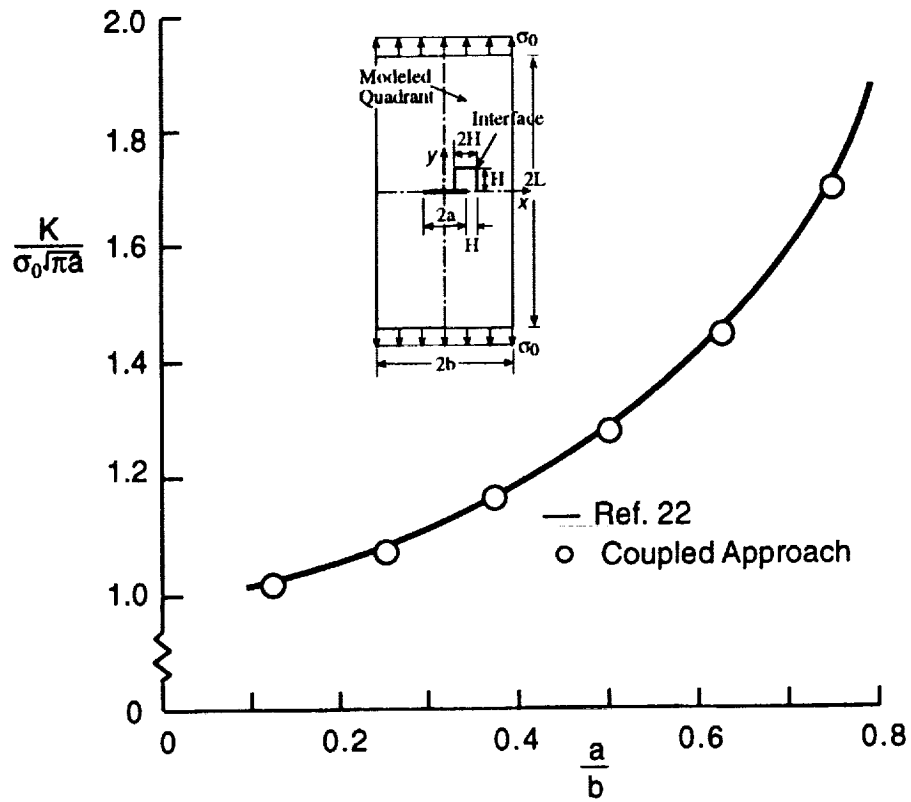


Figure 10. Stress Intensity Factor for Plate with Central Crack, ($\frac{H}{b} = 0.125$).

**Model 1**

**Model 2**

**Model 3**

Interface

Interface

**Model 4**

Blow-up of the local model

Refinement of model necessary

Existing model adequate

Refinement based on the energy norm of the error with a tolerance of 5%.

Interface
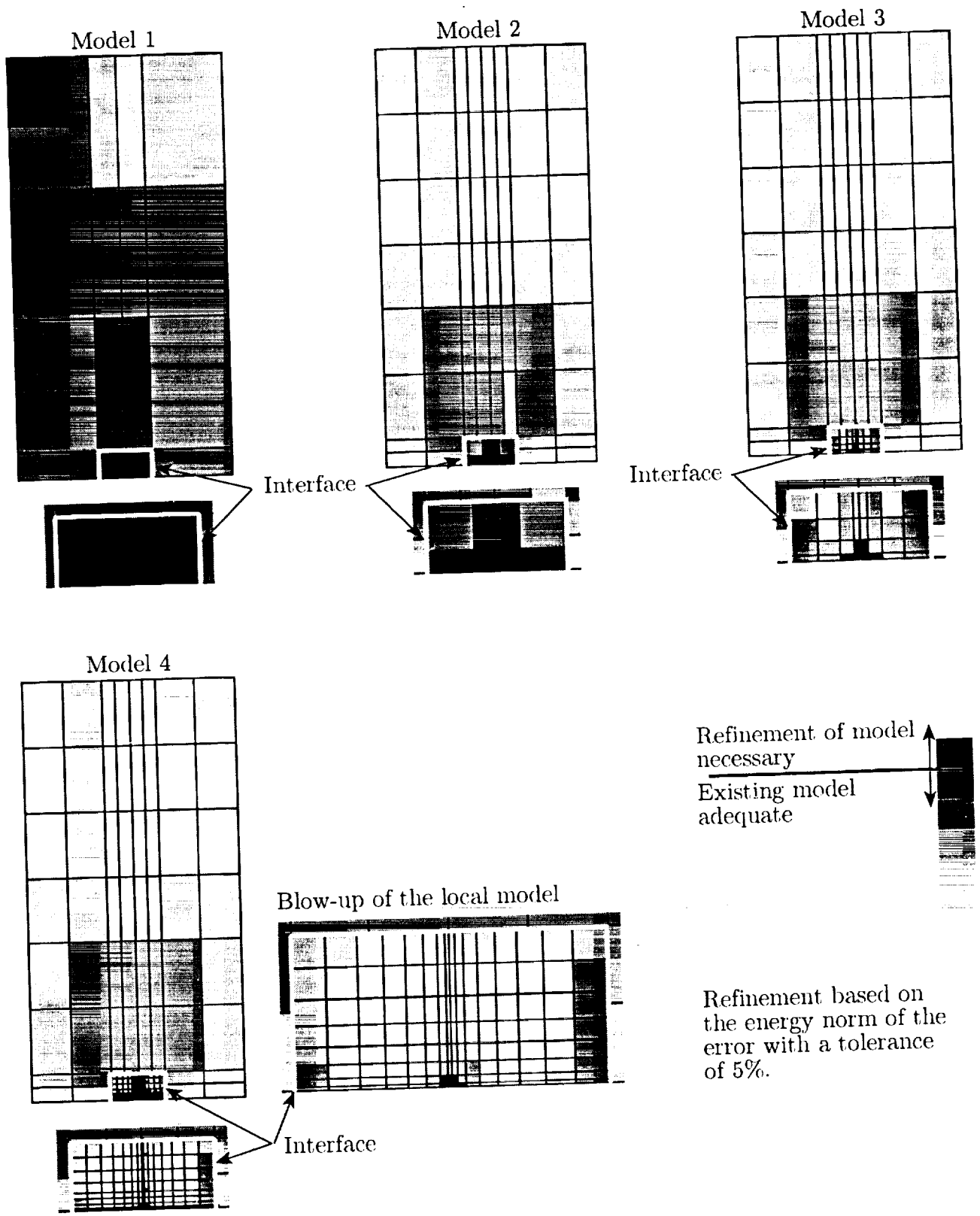
Figure 10. Refinement Indicators for Finite Element Models 1 through 4.
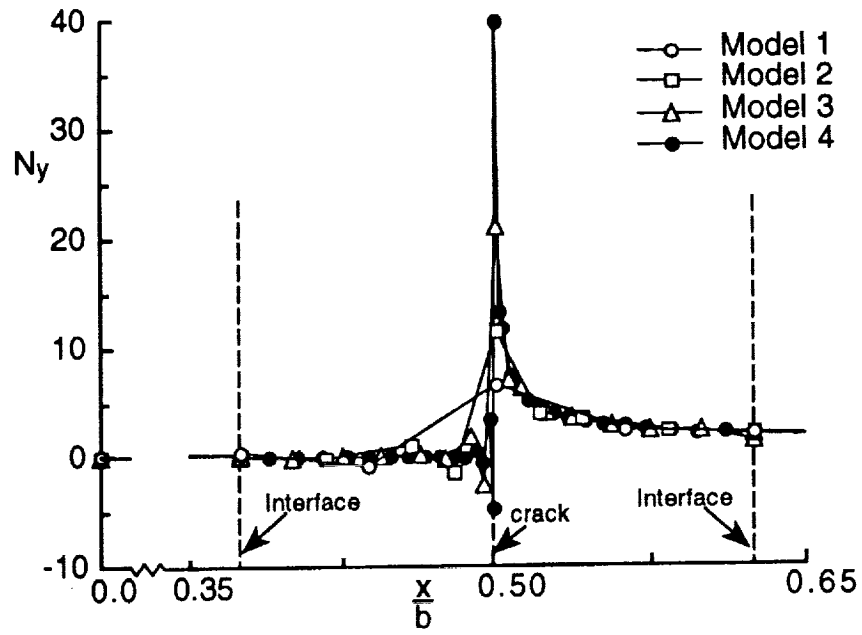
Figure 12. Transverse In-plane Stress Resultant, $N_y$, Distributions.
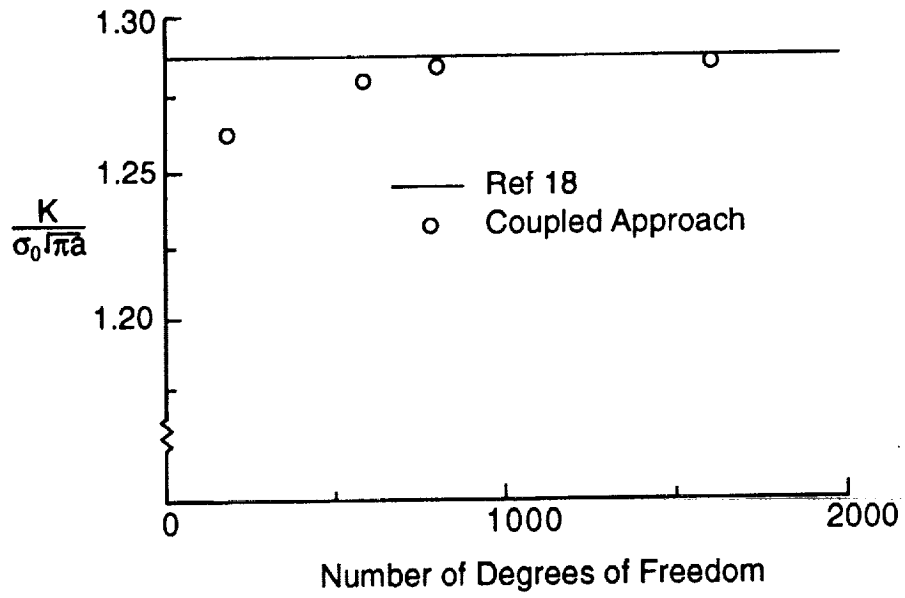
Figure 13. Effect of Model Refinement on the Stress Intensity Factor, $K$.

# REPORT DOCUMENTATION PAGE

| 1. AGENCY USE ONLY (Leave blank) | 2. REPORT DATE <br> August 1992 | 3. REPORT TYPE AND DATES COVERED <br> Technical Memorandum |
|---|---|---|

**4. TITLE AND SUBTITLE**
Computational Methods for Global/Local Analysis

**5. FUNDING NUMBERS**
505-63-53-01

**6. AUTHOR(S)**
Jonathan B. Ransom, Susan L. McCleary,
Mohammad A. Aminpour & Norman F. Knight, Jr.

**7. PERFORMING ORGANIZATION NAME(S) AND ADDRESS(ES)**

NASA Langley Research Center
Hampton, VA 23681

**8. PERFORMING ORGANIZATION REPORT NUMBER**

**9. SPONSORING / MONITORING AGENCY NAME(S) AND ADDRESS(ES)**

National Aeronautics and Space Administration
Washington, DC 20546-0001

**10. SPONSORING / MONITORING AGENCY REPORT NUMBER**

NASA TM-107591

**11. SUPPLEMENTARY NOTES**

Ransom: Langley Research Center, Hampton, Virginia; McCleary: Lockheed Engineering & Sciences Company, Hampton, Virginia; Aminpour: Analytical Services & Materials, Inc., Hampton, Virginia; Knight: Clemson University, Clemson, South Carolina.

**12a. DISTRIBUTION / AVAILABILITY STATEMENT**

Unclassified - Unlimited

Subject Category 39

**12b. DISTRIBUTION CODE**

**13. ABSTRACT (Maximum 200 words)**

Computational methods for global/local analysis of composite structures including both uncoupled and coupled global/local analysis methods are described. In addition, global/local analysis methodology for automatic refinement of incompatible global and local finite element models is developed. Representative structural analysis problems are presented to demonstrate the multilevel analysis methods.

**14. SUBJECT TERMS**
Multilevel Analysis, Global/Local Analysis, Detailed Stress Analysis, Independent Modeling, Automatic Refinement

**15. NUMBER OF PAGES**
23

**16. PRICE CODE**
A03

| 17. SECURITY CLASSIFICATION OF REPORT <br> Unclassified | 18. SECURITY CLASSIFICATION OF THIS PAGE <br> Unclassified | 19. SECURITY CLASSIFICATION OF ABSTRACT | 20. LIMITATION OF ABSTRACT |
|---|---|---|---|